PNAS RESEARCH ARTICLE | GENETICS

Network-based genetic monitoring of landscape fragmentation

Ohad Peled[a], Jaehee Kim[b], and Gili Greenbaum[a,1]

Edited by Marcus Feldman, Stanford University, Stanford, CA; received June 25, 2025; accepted January 21, 2026

Habitat fragmentation is one of the most immediate and substantial threats to biodiversity, generating isolated populations with reduced genetic diversity. Genetic monitoring has become essential for detecting fragmentation and tracking its progress. However, the coherent interpretation of genetic monitoring data and understanding the genetic consequences of fragmentation require frameworks that accurately represent real-world complexity. Existing theoretical frameworks typically rely on simplified spatial structures and do not adequately capture the heterogeneous migration patterns of natural populations. Here, we integrate network theory and mathematical population genetics to develop a framework for studying the genetic consequences of fragmentation processes, explicitly accounting for heterogeneous connectivity and temporal dynamics. We apply this framework to examine how different fragmentation processes affect genetic measures commonly used in genetic monitoring. Through analysis of simulated and empirical networks, we find that different fragmentation scenarios produce substantially distinct trajectories in key genetic measures, sometimes exhibiting rapid transitional dynamics. Furthermore, fragmentation can cause deviations from classical theoretical expectations, such as the expected correlation between genetic and geographic distance (isolation-by-distance) or between genetic diversity and connectivity. Finally, we propose and demonstrate detectable early warning signals in genetic monitoring data that precede rapid transitional phases. Our framework thus provides a practical interpretation of genetic monitoring data, and a proof-of-concept that bridges the gap between idealized theoretical models and real-world connectivity dynamics.

population genetics | fragmentation | network theory | early warning signals

Significance

Landscape fragmentation threatens the persistence of species worldwide. Genetic monitoring is often used to track the genetic health of populations, but the relationship between real-world landscape connectivity and genetic measures remains difficult to model. Here, we integrate network theory with mathematical population genetics to develop a framework that addresses this challenge and enables interpretation of genetic measures along fragmentation processes in networks. We show that different fragmentation scenarios can generate qualitatively different genetic outcomes and violate classical population genetic principles. We also demonstrate that our approach can be used to identify early warning signals in genetic monitoring data before populations suffer significant declines in genetic health. Our framework bridges population genetic theory and conservation practice.

Rapid human-induced environmental changes affect ecological and evolutionary processes, driving biodiversity loss (1, 2). One of the main factors driving these changes is landscape fragmentation, the partitioning of landscapes into small and weakly connected habitat patches (3). Fragmentation reduces connectivity among populations, constraining gene flow and dispersal of individuals (4), which can negatively impact the health and viability of populations (5–7). Landscape fragmentation is expected to erode within-population genetic diversity and increase between-population genetic differentiation due to reduced gene flow and increased genetic drift (8, 9). Decreased genetic diversity can, in turn, reduce population viability in the short term by increasing risks of inbreeding depression (8, 10), while also limiting long-term evolutionary potential and adaptive capacity in response to future environmental changes (11, 12). Consequently, systematically and coherently tracking fragmentation dynamics and their population-genetic consequences through genetic monitoring remains a major goal in conservation biology (2).

Genetic monitoring of population genetic metrics over time is a cost-effective and direct approach for tracking both the genetic impacts and the underlying ecological processes of fragmentation. The alternative, tracking individual movement among habitat patches, is usually resource-intensive and offers only an indirect proxy for the genetic and evolutionary consequences of fragmentation. Consequently, genetic monitoring of wild populations is commonly used to assess population health and viability, landscape connectivity, and species responses to environmental disturbances (2, 13–15). However, evaluating the extent to which fragmentation affects population-genetic metrics, and hence the interpretation of genetic monitoring data, remains a major challenge.

Early theoretical work in population genetics established frameworks for linking genetic diversity and differentiation to migration under simplified assumptions about gene flow patterns and spatial configurations [e.g., the island model, the stepping stone model (16, 17)]. These models provided fundamental insights into how spatial connectivity shapes population genetic structure and introduced key concepts such as isolation-by-distance, where genetic differentiation increases with geographic distance (18), isolation-by-resistance, where differentiation increases with the cumulative

Author affiliations: [a]Department of Ecology, Evolution and Behavior, The Hebrew University of Jerusalem, Jerusalem 9190401, Israel; and [b]Department of Computational Biology, Cornell University, Ithaca, NY 14850

Author contributions: O.P., J.K., and G.G. designed research; O.P. performed research; O.P. analyzed data; and O.P., J.K., and G.G. wrote the paper.

The authors declare no competing interest.

This article is a PNAS Direct Submission.

[1]To whom correspondence may be addressed. Email: gil.g@mail.huji.ac.il.

This article contains supporting information online at https://www.pnas.org/lookup/suppl/doi:10.1073/pnas.2515033123/-/DCSupplemental.

Published February 18, 2026.

landscape resistance between populations by accounting for the difficulty of movement along migration routes (19), and the connectivity–diversity relationship, in which populations that are more connected are expected to exhibit higher genetic diversity (20). However, simplified assumptions of most models limited their practical applicability for genetic monitoring and for evaluation of the impact of fragmentation (21). For example, these models are not suitable to capture the temporal dynamics of fragmentation, where connectivity loss occurs as heterogeneous, sequential processes shaped by the specific spatial and temporal characteristics of anthropogenic or climatic drivers (22). The lack of a modeling framework that integrates realistic spatiotemporal patterns of connectivity and fragmentation thus restricts the practical application of population genetic theory in conservation efforts.

A promising approach for incorporating gene flow patterns into population genetic theory is to represent connectivity between populations as a network—a mathematical construct comprising nodes (habitat patches) connected by edges (connectivity) (23). Population networks can accommodate complex connectivity patterns beyond the scope of classical population genetics models. Several methods have been developed to infer population connectivity from genetic data, either by quantifying differentiation between population pairs to build a network (24–26), or by inferring heterogeneous migration rates across a spatial graph [e.g., EEMS (27, 28)], with applications across a wide range of taxa (29–33). These network-based approaches provide a rigorous framework for modeling realistic fragmentation dynamics. A particularly useful model for population networks is the Random Geometric Graph (RGG) model (34, 35), which models connectivity as being associated with geographical proximity, a basic null-assumption in ecology that is well-aligned with the population genetic concept of isolation-by-distance.

In this work, to bridge the gap between theory and practice, we develop a framework based on population networks, integrating advances in population-genetic theory and network science to investigate the spatiotemporal genetic consequences of landscape fragmentation. This framework explicitly incorporates real-world complexities within a conceptually simple and tractable model. We apply this framework to examine how different fragmentation scenarios affect genetic measures and to assess how network structure impacts population resilience under connectivity loss. This proof-of-concept enables improved interpretation of genetic monitoring data which can facilitate the measurement of fragmentation progression.

Results

To model the genetic consequences of fragmentation, we consider a metapopulation in which some populations are connected by migration. For tractability, we assume equal population sizes and equal migration rates among all connected populations (but we later examine the robustness of our results to violation of these unrealistic assumptions). Any such connectivity pattern can be represented as a population network (Fig. 1*A*). To relate migration patterns to genetic measures, we employ the approach developed by Alcala et al. (36), which consists of two transformations: i) from migration matrices to pairwise coalescent-time matrices (*SI Appendix*, Eqs. **S1** and **S2**) (37), and ii) from coalescent-time matrices to pairwise genetic differentiation measured by F_{ST} (38) (*SI Appendix*, Eq. **S3**; see *Materials and Methods* and *SI Appendix*, Text). This procedure provides, for a given migration matrix, expected pairwise F_{ST} between all population pairs, as well as genetic diversity measured by expected heterozygosity (H_e) for each population (Fig. 1*A*). For simplicity, we further assume uniform mutation rates across all populations, allowing us to use an "unscaled" heterozygosity measure (*SI Appendix*, Eq. **S2**; see *Materials and Methods*); therefore, our H_e values should be interpreted only relatively, and values exceeding one are possible.

To simulate an ecologically plausible metapopulation, which is usually embedded in a geographic landscape, we use a random geometric graph (RGG) model (34, 35) as the initial network. In this model, populations are more likely to be connected if they are geographically close to each other. This model, while generating topologies with specific properties, is well suited for studying population networks because it captures the fundamental ecological constraint that connectivity is typically higher between geographically proximate populations. We model a fragmentation process by iteratively removing edges according to one of several predefined fragmentation scenarios (Fig. 1*B*). After each edge removal, we recompute genetic measures, tracking their changes until all edges have been removed and the network has become fully fragmented into isolated populations. This modeling framework is highly flexible and enables the study of diverse connectivity patterns and fragmentation scenarios while providing rigorous analytical expectations for key genetic measures commonly used in genetic monitoring.

We consider eight fragmentation scenarios (Fig. 1*B*): i) random fragmentation, representing global environmental changes (e.g., climate change); ii) autocorrelated fragmentation, representing spatially correlated landscape disturbances (e.g., agricultural expansion); iii) intrusive fragmentation, representing the emergence of isolated habitats within the landscape; iv) regressive fragmentation, representing the expansion of a disturbance into a natural landscape (e.g., urban expansion); v) distance-based fragmentation, representing reduced dispersal ability through a nonhabitable matrix (e.g., disturbances hindering dispersal through the matrix, reducing dispersal distances); vi) divisive fragmentation, representing linear destruction of connectivity (e.g., road or railway construction); vii) best-case fragmentation, an idealized scenario that sequentially removes the least important edges, thus maximizing connectivity at each step; and viii) worst-case fragmentation, similar to the best-case scenario, except the most important edge is removed at each step. The last two scenarios are theoretical constructs intended to establish upper and lower bounds for genetic measures rather than to depict realistic fragmentation processes. Detailed descriptions of each fragmentation scenario are provided in *Materials and Methods*.

Genetic Monitoring Measures Strongly Depend on the Fragmentation Scenario. Across all fragmentation scenarios, we observe an increase in genetic differentiation and a decrease in genetic diversity as fragmentation progresses (Fig. 2 and *SI Appendix*, Figs. S1 and S2). However, the rate and pattern of these changes vary substantially among scenarios; a similar pattern was observed in networks generated from empirical data (Fig. 3) and using alternative network models (*SI Appendix*, Fig. S3). The best-case scenario consistently retains the highest genetic diversity and the lowest differentiation, as expected (pink curve in Figs. 2 and 3), and the worst-case scenario was the most sensitive to fragmentation (gray curve in Figs. 2 and 3). Thus, these two theoretical extremes provide upper and lower bounds for the retention of genetic health in the metapopulation, against which other fragmentation scenarios can be compared.

In the random and autocorrelated scenarios, the loss of diversity and increase in differentiation are almost undetectable at low fragmentation levels but then become substantial at ~60% fragmentation (blue and orange curves in Fig. 2). This pattern is

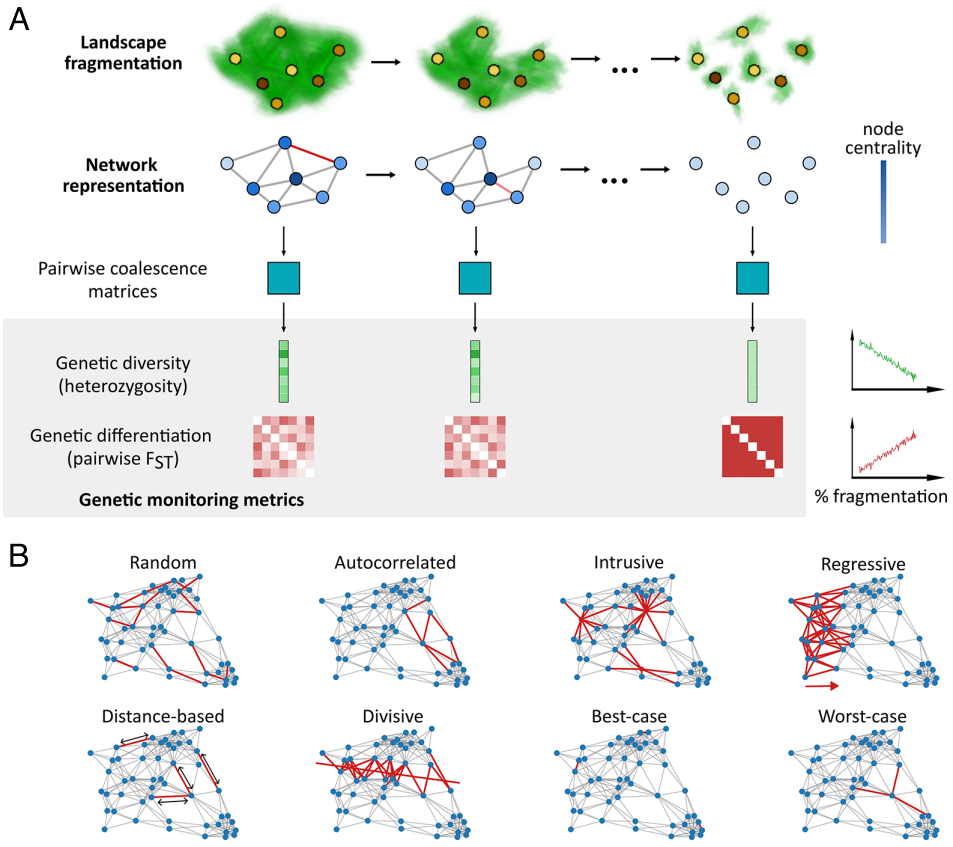

Fig. 1. Schematic representation of the network-based framework for modeling population genetic effects of fragmentation. (*A*) Computation of genetic measures along fragmentation. In the *Top* row, populations (yellow/brown patches) are embedded in a landscape (green) undergoing fragmentation. *Below*, the metapopulation is represented as a network with nodes (blue) denoting populations and edges representing migration between populations. The color intensity of each node denotes its centrality in the network. Fragmentation is simulated by iteratively removing edges (red). A coalescence matrix is derived from each network, which enables the calculation of genetic diversity and differentiation at each fragmentation step (grey box). These metrics allow monitoring of population genetic changes as fragmentation increases (*Right* side of the gray box). (*B*) Modeling fragmentation processes. Illustrated are eight fragmentation scenarios applied to a single realization of a random geometric graph (RGG). Edges removed under each scenario are shown in red. Further details of each scenario are provided in the text.

reflected in concave curves for genetic diversity and convex curves for differentiation. The distance-based scenario (purple curve in Fig. 2) shows a similar trend, but the loss of genetic diversity begins at earlier stages of fragmentation compared to the random and autocorrelated scenarios. In contrast, in the regressive and divisive scenarios, the curvature patterns are reversed: The genetic diversity curve is convex, with steep and substantial decreases in genetic diversity in the early stages of the fragmentation process, and the genetic differentiation curve is concave, indicating earlier deterioration of metapopulation genetic health compared to the other scenarios. For example, in the divisive scenario, a change of >50% in genetic measures occurs after only 25% of the fragmentation process (brown curve in Fig. 2). In the intrusive scenario, both genetic measures change approximately linearly as fragmentation progresses (green curve in Fig. 2).

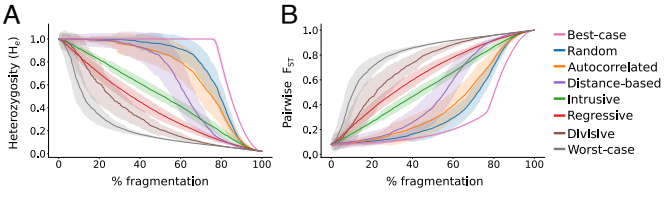

Fig. 2. Changes in genetic measures along fragmentation under eight fragmentation scenarios. (*A*) Mean genetic diversity (H_e) across all populations along fragmentation. (*B*) Mean genetic differentiation (pairwise F_{ST}) among all population pairs. Lines denote means across 100 simulation replicates, with shaded regions indicating SDs. Fragmentation is measured as the fraction of edges removed from the initial network.

To assess robustness, we examined how F_{ST} and H_e measures change along fragmentation while varying key parameters of the model. Specifically, we evaluated i) different initial network topologies, ii) different migration rates, iii) nonequal migration rates, and iv) nonequal population sizes. Although this robustness analysis is not fully comprehensive, given the size of the space of possible population networks, it examines whether our results are a special case of purely mathematical interest or whether they could be relevant to nonidealized real-world populations that surely violate some of the model assumptions. While the RGG model is, arguably, the most relevant baseline model for population networks, our results show that with different initial network topologies (either the Erdős-Rényi model or a small-world network model) the differences among fragmentation scenarios were less pronounced than for RGG (*SI Appendix*, Fig. S3 *A* and *B*). Similarly, when varying the distance threshold cutoff of the RGG model (d), we observe similar differences among fragmentation scenarios, but the variation across replicates was larger for lower d values (*SI Appendix*, Fig. S3 *C* and *D*). In our analysis of three empirically derived networks, results were broadly consistent with the RGG baseline, but the distance-based fragmentation scenario seemed more detrimental, in terms of erosion of genetic diversity and increase in genetic differentiation,

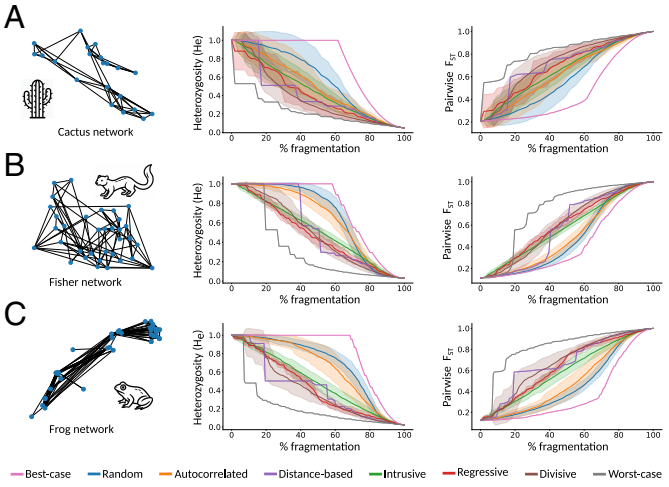

Fig. 3. Changes in genetic measures along fragmentation for empirical population networks. Each panel shows changes in H_e (*Middle*) and pairwise F_{ST} (*Right*) for simulated fragmentation scenarios, with initial network generated from empirical data (*Left*). (*A*) A population network of a Sonoran desert cactus (*Lophocereus schottii*) metapopulation ($K = 21$ populations) from ref. 24. (*B*) A population network of a Fisher (*Pekania pennanti*) metapopulation ($K = 34$) from ref. 30. (*C*) A population network of an Eastern spadefoot toad (*Pelobates syriacus*) metapopulation ($K = 43$) from ref. 29. Lines denote means across 100 simulation replicates, with shaded regions indicating SDs; the distance-based, best-case, and worst-case fragmentation scenarios are deterministic for a fixed network, and therefore no variation is shown.

than in the RGG case (Fig. 3). With different migration rates ($M = 0.2$, $M = 1$, $M = 5$), the patterns of change along fragmentation are similar except that at low migration rates the absolute values of F_{ST} are higher at low levels of fragmentation, as expected (*SI Appendix*, Fig. S4). Nonequal migration rates and population sizes do not seem to have much impact on how mean F_{ST} and H_e change along fragmentation (*SI Appendix*, Figs. S5 and S6), but the variance of both measures increases for higher variance of population sizes (*SI Appendix*, Fig. S7). This implies that when the assumption of equal population sizes is violated, the differences between trends of genetic measures become more difficult to discern.

Overall, our results demonstrate that for a given level of connectivity loss, the level of genetic diversity and between-population differentiation strongly depend on the type of fragmentation process experienced by the metapopulation. This result is robust to various violations of our assumptions and different parameterizations. Therefore, the interpretation of genetic monitoring data must account for the context and drivers of fragmentation. Because it is not always possible to generalize as to the impact of each fragmentation scenario on genetic measures, if possible, evaluations should be made on empirically measured population networks rather than generative network models.

Relationship Between Heterozygosity and Network Components. When considering the distributions of the genetic measures rather than just their means, we observe that H_e distributions remain largely unimodal throughout the fragmentation process, with a shift toward $H_e = 0$ occurring as isolated nodes accumulate (Fig. 4 *A–C* and *SI Appendix*, Figs. S1 and S8 *A–E*). Similarly, the F_{ST} distributions exhibit increasing bimodality, with density accumulating at $F_{ST} = 1$ as more nodes are separated into different components (a component is a maximal set of nodes all connected by paths; Fig. 4 *D–F* and *SI Appendix*, Figs. S2 and S8 *F–J*). Changes in the shape of these distributions along fragmentation are also reflected in the variance of genetic diversity across populations (Fig. 4*G*): the level of fragmentation that maximizes variance, as well as the maximum variance value, differs among fragmentation scenarios. The increase in H_e variance can make the detection of fragmentation—and genetic health in general—more challenging at intermediate fragmentation levels because more populations will need to be sampled to correctly characterize the genetic diversity state of the metapopulation.

As fragmentation progresses, network structure changes and populations begin to disconnect from the main component (*SI Appendix*, Fig. S9). For example, the steep deterioration in genetic health under the divisive scenario (brown in Fig. 2) can be attributed to the early emergence of medium and small network components, which reduce genetic diversity and increase between-component differentiation (*SI Appendix*, Fig. S9*F*). To better understand the effect of component structure on genetic diversity, we tracked the size of the largest component throughout the fragmentation process (Fig. 4*H*). For densely connected components the heterozygosity of populations should be proportional to the size of the component and reflect component's effective population size (39). Indeed, we observe a strong correlation between the size of the largest component and the mean H_e across populations in the network ($r = 0.97$ to 0.98 across scenarios, P-value < 0.001). This correlation is relatively consistent across different fragmentation scenarios, indicating that the size of the largest component is an important determinant of genetic diversity.

Using Network Metrics in Genetic Monitoring. To better understand how tracking network characteristics can inform genetic monitoring, we evaluated the association between genetic measures and commonly used network metrics. We first examined the relationship between a population's genetic diversity and its centrality. There are different ways to measure network centrality (40), each of which can be interpreted differently with respect to population genetic processes (23). Here, we evaluated two common metrics: degree centrality (i.e., the number of edges incident to a node), which measures local centrality, and betweenness centrality (i.e., the frequency with which a node lies on shortest paths between other nodes), which measures global centrality. Under classical population genetics theory, populations with higher connectivity should exhibit greater genetic diversity due to increased gene flow, leading to higher H_e at migration-drift equilibrium (20). Consistent with this expectation, analysis of the initial (prefragmentation) networks showed a strong positive correlation between degree centrality and H_e ($r = 0.71$ to 0.95, Fig. 5*A*). However, because all populations had a relatively high H_e, this relationship was nonlinear, exhibiting a saturating effect: while H_e increased with degree at low connectivity, it plateaued for highly connected nodes (*SI Appendix*, Fig. S10*A*). Hence, local connectivity increases genetic diversity only up to a threshold, beyond which additional migration corridors do not significantly contribute to maintaining genetic diversity. In contrast, the association between H_e and betweenness centrality was weaker for nodes with low betweenness (*SI Appendix*, Fig. S10*B*).

Throughout fragmentation, the correlation between H_e and degree centrality remains consistently high for some scenarios but declines in the later stages of the fragmentation process under the worst-case, divisive, and distance-based scenarios (Fig. 5*A*). This decline may result from network partitioning into components of varying size in these fragmentation scenarios, where component size has a stronger effect on H_e than does local connectivity. For example, a densely connected population in a small component with few populations may have lower H_e than a sparsely connected population in a larger component

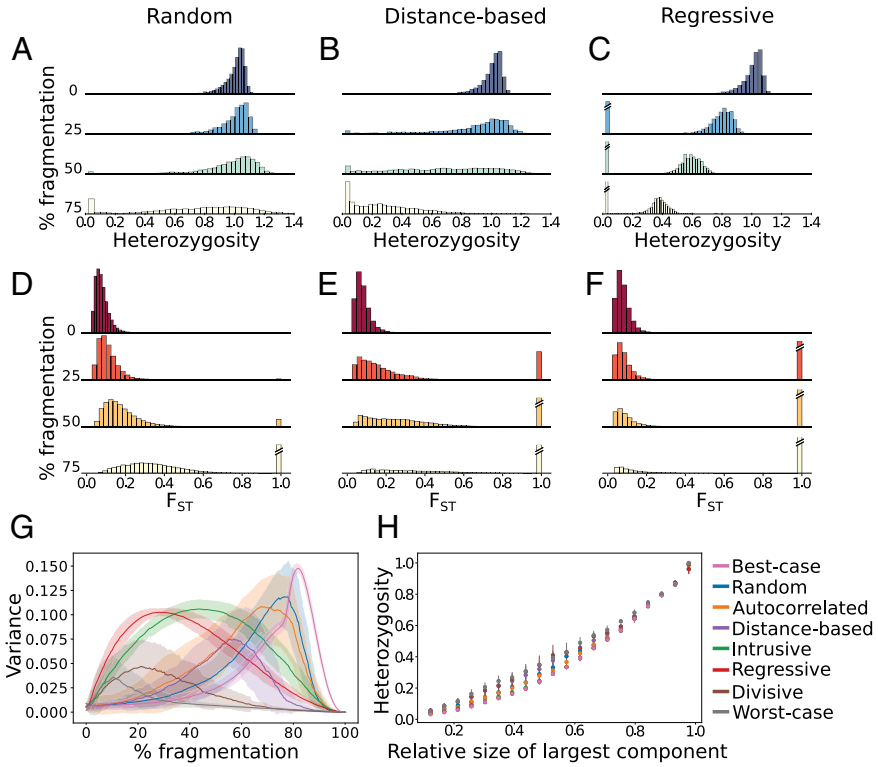

Fig. 4. Changes in the distributions of genetic measures along fragmentation. Panels (*A–F*) show density distributions for three fragmentation scenarios: random, distance-based, and regressive (additional fragmentation scenarios are shown in *SI Appendix*, Fig. S8). Four snapshots from the process are shown: 0%, 25%, 50%, and 75% fragmentation. Diagonal lines on bars indicate truncated values (for $H_e = 0$ or $F_{ST} = 1$). All distributions are pooled from 100 simulation replicates. (A–C) Distribution of expected heterozygosity (H_e) of populations. (*D–F*) Distribution of pairwise F_{ST} across all population pairs. (*G*) Change in the variance of H_e across all populations in the network. (*H*) Relationship between the fraction of nodes in the largest component and mean H_e across all populations in each network. For each scenario, dots denote the means across 100 simulation replicates, and lines denote the SDs.

with many populations. Thus, component size, rather than degree centrality, is a primary determinant of genetic diversity at these intermediate fragmentation stages. Interestingly, in these scenarios, the correlation later rebounds, converging to levels similar to those of the other fragmentation scenarios. This suggests that once components reach comparatively small sizes, within-component degree centrality once again becomes a strong determinant of H_e.

The association between genetic diversity and betweenness centrality was generally weaker than that for degree centrality, with less variation among fragmentation scenarios (Fig. 5*B*). This suggests that populations do not necessarily need to occupy a key gene flow hub to maintain high genetic diversity, as has been observed in some systems (41). One implication of this is that peripheral populations in large, well-connected networks can maintain genetic diversity comparable to that of central populations in smaller, less connected components.

Next, we examined the relationship between pairwise F_{ST} and four network distance metrics relevant for genetic monitoring (Fig. 5*C*): i) Euclidean distance in the two-dimensional space of the embedded RGG network, ii) shortest-path distance [the minimum number of edges required to connect a pair of nodes (42)], iii) random-walk distance [the expected number of edges traversed in a random walk between two nodes (43)], and iv) resistance distance (19), which considers all possible pathways connecting population pairs. Euclidean distance represents the geographic distance, which is often readily available, whereas estimating the network distances requires knowledge of migration patterns in the metapopulation (23). Prior to fragmentation, we observed strong correlations between F_{ST} and all distance metrics ($r = 0.7$ to 1.00, Fig. 5 *D–G* and *SI Appendix*, Fig. S10 *C–F*), indicating that geographically distant populations are more genetically differentiated irrespective of how distance is measured. This finding aligns with the isolation-by-distance and isolation-by-resistance expectations, suggesting that such idealized models are a good approximation for sufficiently well-connected networks (23). However, as fragmentation progresses, these correlations may vary over the course of fragmentation (Fig. 5 *D–G*).

Across all distance matrices, the worst-case and divisive scenarios exhibit consistently lower correlations as fragmentation proceeds. Because these processes split the network into smaller components, the decline likely reflects component-size effects on the correlation estimates. Interestingly, for Euclidean distance, the correlation declines also under the best-case, random, and autocorrelated scenarios (Fig. 5*D*); these scenarios have different effects on network structure (*SI Appendix*, Fig. S9), suggesting that some unknown topological properties are needed to account for the relationship between genetic differentiation and geographic distance. In contrast, for shortest-path distance, the correlation consistently increases across some processes we examined (the theoretical best-case scenario is the exception) (Fig. 5*E*). For the random-walk distance, the relationship remains relatively stable throughout fragmentation for most scenarios (Fig. 5*F*). Resistance distance consistently outperformed other metrics, with the correlation remaining very high throughout fragmentation, except during the worst-case and divisive scenarios (Fig. 5*G*). This is consistent with previous studies under the isolation-by-resistance framework which showed that this metric is a good proxy for pairwise F_{ST} (19). When relaxing the assumptions of equal migration rates and population sizes, results

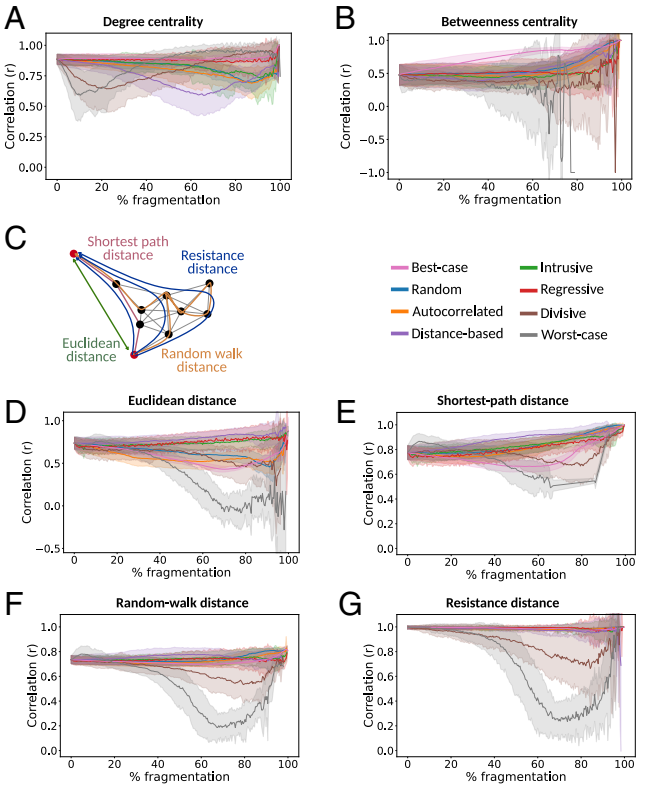

Fig. 5. Correlation between population genetic measures and network metrics. The Pearson correlation coefficient r was computed between genetic diversity (H_e) and network centrality (*A* and *B*), or between genetic differentiation (F_{ST}) and distance metrics (*D*–*G*), for eight fragmentation scenarios. (*A*) Correlation between a population's H_e and its degree centrality (number of connected edges). (*B*) Correlation between a population's H_e and its betweenness centrality (global centrality metric). (*C*) Schematic illustration of four different distance metrics for a pair of populations (red nodes). (*D*) Correlation between the F_{ST} of a pair of populations and their Euclidean distance in the two-dimensional space in which the RGG network is embedded. (*E*) Correlation between the F_{ST} of a pair of populations and their shortest-path network distance. (*F*) Correlation between the F_{ST} of a pair of populations and their random-walk network distance. (*G*) Correlation between the F_{ST} of a pair of populations and their resistance distance.

remain consistent except for minor changes in the divisive and worst-case scenarios (*SI Appendix*, Figs. S11 and S12).

Overall, these analyses highlight that the topological properties of population networks can inform the tracking of genetic diversity and differentiation patterns. However, relating genetic measures to network properties such as components, centrality, or distance measures should, in most cases, be done in the context of the fragmentation scenario. Classical population genetic relationships—such as those between gene flow and diversity or distance and differentiation—are useful for well-connected populations but may diverge from classical theory when fragmentation processes shape the topology of metapopulation connectivity.

Early Warning Signals in Genetic Monitoring. The goal of genetic monitoring is to track the genetic health of populations and to infer underlying ecological processes. However, our findings suggest that inferring fragmentation solely from genetic metrics can be challenging because substantial shifts in genetic measures often occur only in the later stages of the fragmentation process under certain fragmentation scenarios. In such cases, once genetic diversity declines and population differentiation increases, the transition is both rapid and pronounced (Fig. 2). This transition can be considered a tipping-point phase, before which it is difficult to detect ongoing fragmentation by tracking the means of H_e and F_{ST}. This raises the question: Can genetic monitoring data detect landscape fragmentation early enough—before the population transitions to a highly fragmented and diversity-depleted state? In other words, if we are tracking genetic measures in a metapopulation that is progressively undergoing fragmentation, can we use genetic data to provide an early warning signal prior to the tipping-point phase during which genetic diversity and differentiation dramatically change? To address this question, we evaluated whether early warning signals can be extracted from genetic diversity measures, borrowing methods from complex systems theory (44, 45). Our analysis provides proof-of-concept for the potential to integrate early warning methodologies into genetic monitoring frameworks.

For this demonstrative analysis, we focused on the genetic diversity under the autocorrelated fragmentation scenario, where edges are removed in a spatially coordinated manner. We first considered a genetic monitoring scheme that tracks the H_e distributions of all populations throughout fragmentation (Fig. 6*A*). At each fragmentation step, we analyzed the distribution of H_e across populations and computed several summary statistics—SD, skewness, and kurtosis—which have been found to be reliable early warning indicators in other disciplines (46, 47). Another common statistic, lag-1 autocorrelation, was not used because it is intended to measure stability around a single equilibrium (46, 48), which did not hold in our simulations. As the metapopulation approaches the tipping-point phase, the theoretical expectation is that the SD of the H_e distribution will increase, the skewness will shift toward the new state (in this case, asymmetry toward lower H_e values), and the kurtosis will change due to an increased frequency of extreme values (45, 47). Because their interpretation depends on the baseline distribution, consistent changes in skewness or kurtosis, regardless of sign, can indicate proximity to a transition. To evaluate this, we computed these summary statistics throughout fragmentation (green curves in Fig. 6 *B*–*D*) and examined whether they show substantial changes prior to the tipping-point phase (the sharp drop in the orange curves at ∼ 80–90% fragmentation in Fig. 6 *B*–*D*).

Some early warning signals prior to the tipping-point phase were clearly observable in our analyses (Fig. 6 *B*–*D*). For example, the SD of the distribution of H_e across the metapopulation increases steadily as fragmentation progresses, and substantial changes in this statistic are observable at the early stages of fragmentation even when changes in the mean are not yet detected (Fig. 6*B*). Thus, by tracking the SD among populations as fragmentation increases, a noticeable change in this summary statistic could be identified and used as an early warning signal before the tipping-point phase. The mean skewness and kurtosis also showed early changes that can serve as early warning signals (Fig. 6 *C*–*D*). However, the trajectories of skewness and kurtosis fluctuated as fragmentation increased and were noisier than the SD, suggesting that they are less reliable as early warning indicators. This means that, while tracking the mean metapopulation H_e would not indicate that a rapid reduction in genetic health is approaching, monitoring higher moments could potentially provide an early indication of genetic deterioration. Importantly, the same early-warning is observed in our robustness analysis with varying migration rates (*SI Appendix*, Fig. S13), and is even enhanced with varying population sizes (*SI Appendix*, Fig. S14), suggesting that such signals may not be unique to particular model setups. In the nonequal population size analysis, the initial H_e distribution is more skewed than the equal-sizes scenario.

We also considered a more limited monitoring scenario, where H_e is monitored for a single population (Fig. 6*E*). In this setting, a single population is tracked as fragmentation

increases, and we evaluate the H_e distribution of 25% sliding temporal windows throughout fragmentation. As with the previous scenario, we tracked changes in the summary statistics of the distributions along fragmentation. Unlike the scenario that tracks the entire metapopulation, here we were not able to identify substantial early warning signals (Fig. 6 *F–H*). While the SD did increase as fragmentation progressed, the change was not substantial prior to the tipping-point phase (Fig. 6*F*). Although no directional change in kurtosis was observed, skewness showed a moderate early increase, which could potentially provide some early warning (Fig. 6 *G* and *H*).

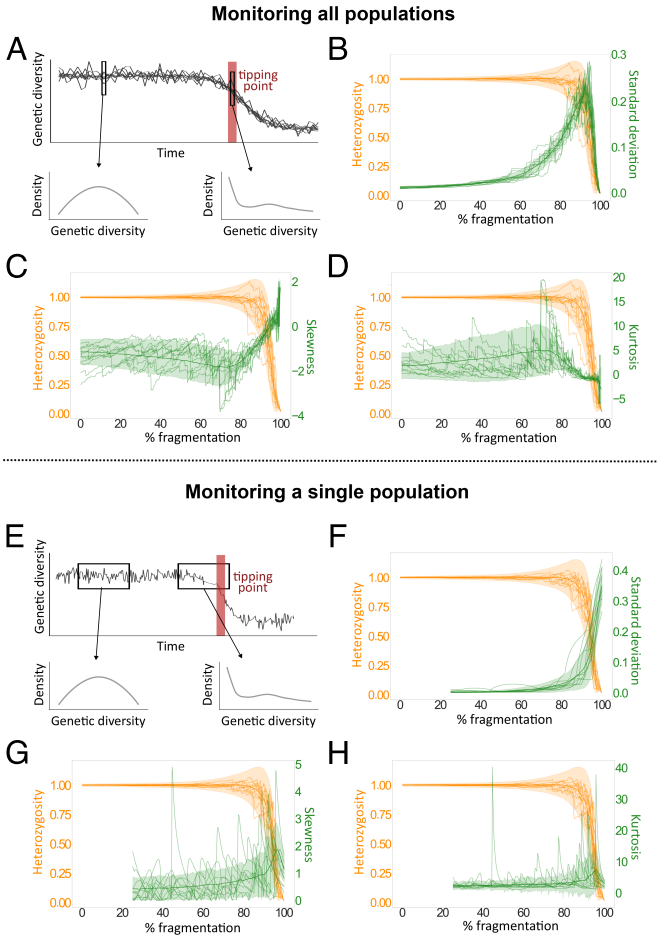

Fig. 6. Early warning signals before tipping point in genetic monitoring. The analysis examines fragmentation under the autocorrelated scenario (Fig. 1*B*). (*A*) Schematic of the metapopulation-monitoring approach. At each fragmentation step, we analyze the He distribution of all connected populations in the network (largest component). The tipping-point phase, during which genetic diversity dramatically declines, is denoted in red. Genetic diversity distributions closer to the tipping-point phase may differ, with summary statistics potentially providing early warning. (*B–D*) Mean metapopulation heterozygosity (orange) and three early warning statistics [green: SD in (*B*), skewness in (*C*), and kurtosis in (*D*)] along fragmentation. Solid lines show the mean across 100 simulation replicates, shaded areas show the SD, and thin lines show ten individual replicates. (*E*) Schematic of the single population monitoring approach. The He of a single population is tracked with a sliding window; the He distributions in each window are then analyzed. The tipping-point phase is shown in red. As above, the genetic diversity distributions in windows closer to the tipping-point phase may differ, with summary statistics potentially providing an early warning. (*F–H*) Mean single population heterozygosity (orange) and three early warning statistics computed from 25% of the data per window [green: SD in (*F*), skewness in (*G*), and kurtosis in (*H*)]. Solid lines show the mean across 100 simulation replicates, shaded areas show the SD, and thin lines show ten individual replicates.

Taken together, our analyses indicate that under the simulation settings examined, cross-sectional monitoring of multiple populations at each sampling occasion yields earlier and more reliable early warning signals than tracking a single population throughout fragmentation, even when the latter is summarized over an extended temporal window. The likely reason is that the cross-sectional snapshot includes multiple quasi-independent observations per fragmentation step, whereas the sliding-window yields serially autocorrelated records. We observe similar results in our robustness analysis (*SI Appendix*, Figs. S15 and S16).

Discussion

Habitat fragmentation is one of the most pressing threats to global biodiversity (3, 49), and genetic monitoring could be instrumental in tracking and managing it (2). However, developing monitoring and intervention strategies that take into account the real-world complexities of population structure remains a challenge (50, 51). We present a framework that enables the modeling of habitat fragmentation and its impacts on population genetic measures, thereby expanding the potential scope of genetic monitoring. We examined the effects of different fragmentation scenarios on genetic measures, in simulated and empirically derived networks, and found that the same rate of fragmentation can lead to markedly different patterns of genetic differentiation between populations (F_{ST}) and genetic diversity within populations (H_e). Our results suggest that classical population genetic relationships, such as the association between F_{ST} and distance or between gene flow and local genetic diversity, may not always hold. Finally, we demonstrate how genetic monitoring can potentially be used to detect early warning signals before fragmentation triggers critical shifts in the genetic health of populations.

Human activity can induce fragmentation in different ways, but theoretical investigations of fragmentation dynamics and their potential consequences have thus far been limited (22, 52). Our results underscore the importance of considering the sequence of events leading to fragmentation. While we observe steady rates of genetic changes that are consistent with theory in some scenarios (53, 54), we also find cases in which genetic measures change abruptly (Fig. 2). An important factor in shaping the change in genetic measures is the maximum number of connected populations in the network (i.e., the size of the largest component; Fig. 4*H*). This pattern holds even when populations within components are weakly or indirectly connected. From a landscape management perspective, it implies that enhancing connectivity between network modules (i.e., clusters of connected populations) may be more beneficial for maintaining high levels of genetic diversity than increasing direct connectivity within a weakly connected module. This result is consistent with the expectation that larger populations (or metapopulations) will exhibit higher genetic diversity due to increased gene flow and decreased genetic drift at the global scale (39). However, increasing global connectivity can lead to homogenization of genetic pools, potentially leading to adverse effects due to the erosion of local adaptation (55, 56). Considering the spatial scale at which connectivity between populations is measured is also crucial for accurately interpreting genetic monitoring outputs.

Populations and ecological systems facing environmental changes can undergo dramatic, unexpected, and often irreversible transitions. In the context of tracking biodiversity, several studies have introduced the concept of fragmentation thresholds that lead to regime shifts in biodiversity (57–59). However, regime shifts in terms of genetic health and population-level metrics have

received far less attention and have been considered primarily in the context of adaptive evolution in response to stress (60). Consequently, genetic monitoring of populations is often reduced to qualitative assessments. Because fragmentation can lead to rapid shifts in genetic metrics (e.g., random or autocorrelated fragmentation in Fig. 2), a standard interpretation of genetic monitoring—no genetic change over time implies no underlying fragmentation process—can be misleading. As a proof-of-concept, we showed that early warning signals may be detectable by tracking features of the distributions of genetic monitoring data. This is particularly true if a large number of populations in the metapopulation are monitored. Although there is a substantial body of theoretical and statistical literature on early warning signals (44, 45, 48, 61), to the best of our knowledge, no theoretical or empirical studies have explored the integration of these methods with population-genetic data so far. Applying a more comprehensive suite of early warning methods (e.g., Kendall's τ statistic, conditional heteroskedasticity) to empirical data may shed additional light on the effectiveness of this approach.

Patterns of spatial genetic structure have been extensively studied for almost a century, both in theoretical population genetic models (17, 18, 37, 62) and in empirical studies of natural populations (63–65). One prevailing view is that spatial separation and matrix permeability generate isolation-by-distance and isolation-by-resistance patterns, respectively (17–19, 66, 67). However, we find that these patterns may deviate from classical expectations depending on the underlying fragmentation scenario and the distance metric used (Fig. 5 *D*–*G*). Yet, we do find support for previous work suggesting that isolation-by-resistance is a good proxy for genetic differentiation in most cases (19). Similarly, the relationship between genetic diversity and connectivity (68–70), a key guideline in conservation practices (71), can also weaken during fragmentation (Fig. 5 *A* and *B*). These findings highlight the need to integrate complex spatial configurations of populations and realistic descriptions of ecological processes into population genetic studies.

Although our framework is flexible and allows detailed spatial configurations, it does not cover many real world processes (e.g., extinction-recolonization dynamics). While our robustness analyses suggest that the way different fragmentation scenarios affect genetic measures is relatively general, other ecological features may have important impacts. Our main goal, therefore, is to provide qualitative understanding of how genetic monitoring data should be interpreted, rather than to offer precise ways to represent realistic population dynamics. One important assumption in our model relates to the time required for a system to reach migration-drift equilibrium between fragmentation steps. When the rate of fragmentation is substantially faster than the rate of approach to equilibrium, our framework may not be appropriate. It has been suggested that genetic differentiation may respond more rapidly than heterozygosity to changes in migration (53) and reach equilibrium faster (72, 73); therefore, in some cases, the framework may be suitable for tracking genetic differentiation but not genetic diversity.

While genetic monitoring data are increasingly available to conservation practitioners, our results indicate that this information alone is insufficient to reliably infer whether fragmentation is occurring, or to quantify its magnitude, without some knowledge of the underlying fragmentation scenario. An alternative application of the framework presented here is to characterize migration routes between populations, the network edges, using genetic or nongenetic data, and then simulate fragmentation on that network, as we demonstrate in Fig. 3. Once an empirically derived network is available, it is possible to examine the consequence of different types of fragmentation scenarios, and to evaluate the performance of different distance metrics (as in Fig. 5). Thus, rather than replacing fully parameterized demographic models, our network-based approach provides a flexible bridge between topology-only metrics and explicitly parameterized population genetic calculations, matched to the level of information available for a given system.

As population-genomic data become increasingly accessible, genetic monitoring is expected to emerge as a leading tool in conservation biology for assessing the health, ecology, and behavior of wild populations. However, the gap between theoretical expectations and practical challenges in conservation biology currently limits our ability to accurately interpret genetic data and develop landscape-specific and species-specific conservation strategies. Our framework incorporates the real-world complexities of space and time and is readily interpretable in terms of genetic monitoring. Here, we explored an important aspect of fragmentation—the processes and patterns by which between-population connectivity is lost—but our framework can be readily expanded to investigate other anthropogenic effects, such as habitat loss (e.g., by simulating different node-removal processes) or the utility of interventions (e.g., prioritization of ecological corridors). Our network-based framework thus serves to narrow the gap between theoretical insights and the complex ecological realities of conservation biology.

Materials and Methods

All analyses were performed using Python 3.11.1, except where stated otherwise.

Computing Genetic Measures in Population Networks. To compute genetic measures for population networks, we employed the framework developed by Alcala et al. (36), which integrates the mathematical relationship between migration and coalescence times by Wilkinson-Herbots (37) (*SI Appendix*, Eqs. **S1** and **S2**) with the relationship between coalescent times and F_{ST} by Slatkin (38) (*SI Appendix*, Eq. **S3**). Our method relies on transformations among three matrices: i) the migration matrix describing the pairwise migration rates, ii) the coalescence matrix describing the expected time to coalesce for two lineages within or between populations, and iii) the F_{ST} matrix describing the pairwise genetic distance between populations. A full explanation of the derivations and computations is presented in *SI Appendix*, Text.

We considered an idealized system of K populations of equal size N, evolving under the neutral Wright–Fisher model at migration-drift equilibrium (20). Let m_{ij} denote the backward migration rate from population i to j, representing the probability that a lineage in i originated in j in the previous generation. For a pair of populations i and j ($i \neq j$), the weight assigned to the edge is $M_{ij} = 4Nm_{ij}$, representing the expected number of migrants from i to j per generation. We assumed symmetric migration ($m_{ij} = m_{ji}$ for all i and j) to ensure conservative migration (37), where total incoming and outgoing migration balance in each population: $\sum_{j\neq i} M_{ij} = \sum_{j\neq i} M_{ji}$. While conservative migration is a weaker assumption than symmetric migration, we imposed symmetric migration in the main text analyses for tractability (*Robustness Analysis*). Under these assumptions, the migration structure of the populations is represented as a symmetric, undirected network M of K nodes with zero-diagonal entries. We simulated population networks with $K = 50$ nodes, where migration rates are uniform across all edges ($M_{ij} = 1$). All initial networks had a fixed total of 250 edges to reduce variance not attributed to fragmentation.

Simulating Fragmentation Processes in Population Networks. Because natural populations are embedded in a geographic space, we used spatial network models (74), in which nodes correspond to populations with assigned geographic coordinates. We primarily used the random geometric graph (RGG)

model (35), a simple and well-studied spatial network model, to generate the initial network in our simulations (in Fig. 3, we use empirical networks and in *SI Appendix*, Fig. S3 we use alternative network models). In the RGG model, K populations are placed uniformly at random in a unit square in Euclidean space, and an edge is formed between two nodes if their Euclidean distance is below a fixed threshold d. The RGG model is particularly well-suited for representing migration in spatially structured populations because it captures the ecologically realistic constraint that migration occurs only between sufficiently proximate populations. The value of d above which the network is almost surely connected for two-dimensional RGG networks is $\sqrt{\frac{\log K}{\pi K}}$ (34), which equals $d = 0.16$ for $K = 50$. We therefore set $d = 0.3$, which consistently generates a connected network that is moderately dense yet sufficiently above the disconnection threshold (see *SI Appendix*, Fig. S3 *C* and *D* for alternative d parameterization).

To model the fragmentation process, we sequentially remove edges from the initial network, one at a time, until no edges remain. We consider eight fragmentation scenarios (Fig. 1). i) *Random fragmentation*. At each fragmentation step, an edge is removed uniformly at random, representing nonspecific habitat deterioration, such as fragmentation induced by global climate change. ii) *Autocorrelated fragmentation*. Initially, one random edge is removed. At each subsequent step, one edge is removed uniformly at random from the set of edges adjacent to the previously removed edge (i.e., edges sharing a node with the last removed edge). This process models spatially correlated landscape disturbances, such as urban or agricultural expansions. iii) *Intrusive fragmentation*. A node is selected uniformly at random, and all its incident edges are removed in random order. Once these edges are removed, another node is chosen randomly, its incident edges are removed, and the process is repeated. This process generates isolated habitats within the landscape, representing, for example, the formation of microreserves–small, disconnected populations. iv) *Regressive fragmentation*. Edges are sorted by the minimum x-coordinate of their incident nodes in the Euclidean plane and removed progressively from low to high x-coordinate values, starting with the edge having the smallest x-coordinate. This process represents large-scale spatial disturbances moving across the habitat, such as shifts in climate-change fronts. v) *Distance-based fragmentation*. At each step, the edge connecting the most distant populations in the underlying Euclidean space is removed. This process represents a general environmental deterioration that impedes long-distance dispersal among habitat patches. vi) *Divisive fragmentation*. A line is drawn in the Euclidean plane by connecting two points on different boundaries (either opposing or neighboring boundaries) of the metric space (selected uniformly at random), effectively bisecting the habitat. All edges intersecting this line are sequentially removed, starting with those having the smallest x-coordinate [as defined in iv)]. This process models the introduction of linear barriers, such as roads or railways, into the landscape. vii) *Best-case fragmentation*. At each step, the edge with the lowest betweenness centrality is removed. Betweenness centrality was computed using the NetworkX Python library (75). Because such edges contribute minimally to network connectivity, removing them is expected to have the least impact on genetic measures. Although this scenario is not realistic, it serves as an upper benchmark for evaluating genetic measures at a given level of fragmentation. viii) *Worst-case fragmentation*. Similar to best-case fragmentation, but at each step, the edge with the highest betweenness centrality is removed. This process provides a lower benchmark for genetic measures at a given level of fragmentation.

These eight fragmentation processes do not exhaustively cover all possible scenarios, but rather describe typical ecological and anthropogenic disturbance patterns relevant to genetic monitoring (22, 76). Because these processes are stochastic, we performed 100 independent replicates per fragmentation type, randomizing the initial network configuration and the fragmentation sequence in each replicate.

In each simulation replicate, we computed the changes in F_{ST} and H_e distributions in response to fragmentation, assuming migration-drift equilibrium is reached between successive iterations of edge removal. Accordingly, our analyses track genetic measures at a series of quasi-equilibria across increasing fragmentation. Reported "rates" therefore describe population genetic responses across fragmentation levels, not temporal speeds. Each replicate generates a sequence of migration matrices $M_0, \ldots, M_x$, with x being the last fragmentation step. From these migration matrices, we computed corresponding F_{ST} matrices $F_0, \ldots, F_x$ and H_e vectors $H_0, \ldots, H_x$. These sequences reflect the changes in genetic differentiation and genetic diversity throughout fragmentation. Using these sequences, we tracked changes in the means (Fig. 2), sample variances (Fig. 4*G*), and distributions (Fig. 4 *A*–*F*) of the genetic measures along fragmentation. We also tracked the relative size of the largest component in the network to study its relationship with the mean H_e of the network (Fig. 4*H*).

In addition to simulated networks, we examined three empirically derived population networks (Fig. 3): a Sonoran desert cactus (*Lophocereus schottii*) network with $K = 21$ populations (24), a fisher (*Pekania pennanti*) network with $K = 34$ populations (30), and an Eastern spadefoot toad (*Pelobates syriacus*) network with $K = 43$ populations (29). These networks were already inferred from genetic data in these studies.

We also evaluated changes in network structure throughout fragmentation by tracking four structural categories (*SI Appendix*, Fig. S9): i) largest component, ii) other components with >3 populations (medium components), iii) components of 2 to 3 populations (pairs/triads), and iv) isolated nodes. At each fragmentation step, we computed the mean proportion of nodes in each category across simulation replicates.

Correlations Between Genetic Measures and Node Attributes. To investigate how network metrics influence genetic monitoring along fragmentation, we examined the relationship between genetic measures and network metrics. For each network at each fragmentation step, we computed two node centrality measures, degree centrality (number of incident edges for the focal node), and betweenness centrality (how often a node lies on the shortest paths between other pairs of nodes), for all nodes in the network. We then computed the Pearson correlation coefficient (r) between a node's He and its centrality score for each centrality measure (we excluded isolated nodes, for which centrality is undefined). Then, for each one of the centrality metrics and each fragmentation scenario, we computed the mean r and its SD for each fragmentation step across the simulation replicates. We only show significant correlation results ($P < 0.05$) with data from 5 or more replicates.

Similarly, we evaluated the relationships between network distance metrics and pairwise F_{ST}. We computed the distance between all pairs of nodes in each fragmentation step using four distance metrics: i) Euclidean distance, the standard geometric measure in the embedded metric space, analogous to the typical geographic distances among populations; ii) shortest-path distance (least cost path) (42), calculated as the minimum number of edges needed to traverse from one node to another, reflecting topology-aware movement; iii) random-walk distance (mean first-passage time) (43), the expected number of steps for a simple random walker to reach node j from node i for the first time, reflecting uninformed or non-targeted movement (this is an asymmetric distance metric). (23); iv) Resistance distance, a metric derived using circuit theory that is precisely related to the random-walk commute time (the time to travel from one node to another and back), accounting for all possible pathways of gene flow connecting the two nodes (19). The correlations were calculated only within connected components of size >3, and pairs of nodes in disconnected components were excluded from correlation calculations (these pairs have $F_{ST} = 1$ and are infinitely distant from each other for all network distances). We computed the Pearson correlation coefficient (r) between the F_{ST} of all node pairs and their distance score, at each fragmentation step and for each distance metric. For each correlation, we obtained a P-value using a quadratic assignment procedure (QAP) with 1,000 permutations (77). For networks with multiple components, we computed a size-weighted mean of r across components and combined the component-wise $p-values$ using Fisher's method (78). We then computed the mean r and its SD for each fragmentation step across the simulation replicates, for each one of the distance metrics and each fragmentation scenario. We only show significant correlation results ($P < 0.05$) with data from 5 or more replicates.

Detecting Early Warning Signals Before Population Collapse. To identify early warning signals, we computed several summary statistics of the genetic diversity (H_e) distributions that are commonly used as early warning signals:

SD, skewness, and kurtosis. As the process approaches the tipping-point phase, the theoretical expectation is that the SD of the H_e distribution will increase, the skewness will shift toward lower H_e values (higher asymmetry), and increased frequency of extreme values will lead to higher kurtosis (45, 47). We did not use the lag-1 autocorrelation, although it is often used to measure the return rate to equilibrium after a perturbation (46), because this statistic is designed to measure stability around a single equilibrium (46, 48), whereas our framework considers a series of fragmentation events between which the system arrives at migration-drift equilibrium.

For this analysis, we focused on autocorrelated fragmentation (Fig. 2*B*). We used a more connected initial network than used in previous analyses, an RGG with $d = 0.6$, to capture a substantial period that is far from the tipping-point phase. We ran 100 simulation replicates and we considered two monitoring scenarios: i) *entire metapopulation monitoring*, where we analyze the H_e distribution across all populations in the largest component at each step (so as not to introduce bias near zero H_e values from isolated populations), and ii) *single population monitoring*, focusing on the H_e of the final nodes to become isolated. In the latter case, we used the generic_ews function from the R package earlywarnings to apply a sliding window approach as fragmentation increases, with window size of 25% and default parameters without detrending or preprocessing the data.

Robustness Analysis. To evaluate how robust our results are to model assumptions, we repeated the analysis while varying key parameters. Specifically, we examined the effect of changing the i) initial network topology, ii) mean migration rate, iii) variance of migration rates among edges, and iv) variance of population sizes. These procedures are detailed in *SI Appendix*.

Data, Materials, and Software Availability. The code used to generate and analyze the data in this paper is available on GitHub at https://github.com/Greenbaum-Lab/pop_net_fragmentation.git (79). All other data are included in the manuscript and/or *SI Appendix*.

ACKNOWLEDGMENTS. We thank Keith D. Harris and Eyal Halutz for their input and assistance in the analysis. The research was funded by the Binational Science Foundation Grant No. 2021244. O.P. was supported by fellowships from the Israel Ministry of Environmental Protection and from the Minerva Center for the study of Population Fragmentation.

1. P. Jaureguiberry *et al*., The direct drivers of recent global anthropogenic biodiversity loss. *Sci. Adv.* **8**, eabm9982 (2022).
2. S. Hoban *et al*., Global genetic diversity status and trends: Towards a suite of essential biodiversity variables (EBVs) for genetic composition. *Biol. Rev.* **97**, 1511–1538 (2022).
3. N. Haddad *et al*., Habitat fragmentation and its lasting impact on earth's ecosystems. *Sci. Adv.* **1**, e1500052 (2015).
4. H. Van Dyck, M. Baguette, Dispersal behaviour in fragmented landscapes: Routine or special movements? *Basic Appl. Ecol.* **6**, 535–545 (2005).
5. J. Fischer, D. B. Lindenmayer, Landscape modification and habitat fragmentation: A synthesis. *Glob. Ecol. Biogeogr.* **16**, 265–280 (2007).
6. L. Fahrig, Effects of habitat fragmentation on biodiversity. *Annu. Rev. Ecol. Evol. Syst.* **34**, 487–515 (2003).
7. R. Aguilar *et al*., Habitat fragmentation reduces plant progeny quality: A global synthesis. *Ecol. Lett.* **22**, 1163–1173 (2019).
8. D. H. Reed, R. Frankham, Correlation between fitness and genetic diversity. *Conserv. Biol.* **17**, 230–237 (2003).
9. A. Lowe, D. Boshier, M. Ward, C. Bacles, C. Navarro, Genetic resource impacts of habitat loss and degradation; Reconciling empirical evidence and predicted theory for neotropical trees. *Heredity* **95**, 255–273 (2005).
10. D. Charlesworth, J. H. Willis, The genetics of inbreeding depression. *Nat. Rev. Genet.* **10**, 783–796 (2009).
11. A. S. Jump, R. Marchant, J. Peñuelas, Environmental change and the option value of genetic diversity. *Trends Plant Sci.* **14**, 51–58 (2009).
12. S. Manel, R. Holderegger, Ten years of landscape genetics. *Trends Ecol. Evol.* **28**, 614–621 (2013).
13. M. Siol, I. Bonnin, I. Olivieri, J. Prosperi, J. Ronfort, Effective population size associated with self-fertilization: Lessons from temporal changes in allele frequencies in the selfing annual *Medicago truncatula*. *J. Evol. Biol.* **20**, 2349–2360 (2007).
14. K. C. Kendall *et al*., Demography and genetic structure of a recovering grizzly bear population. *J. Wildl. Manag.* **73**, 3–16 (2009).
15. L. Hauser, G. J. Adcock, P. J. Smith, J. H. Bernal Ramírez, G. R. Carvalho, Loss of microsatellite diversity and low effective population size in an overexploited population of New Zealand snapper (*Pagrus auratus*). *Proc. Natl. Acad. Sci. U.S.A.* **99**, 11742–11747 (2002).
16. S. Wright, "The roles of mutation, inbreeding, crossbreeding and selection in evolution" in *Proceedings of the Sixth International Congress of Genetics*, D. F. Jones, Ed. (Brooklyn Botanic Garden, Brooklyn, New York, 1932), vol. 1, pp. 356–366.
17. M. Kimura, G. H. Weiss, The stepping stone model of population structure and the decrease of genetic correlation with distance. *Genetics* **49**, 561 (1964).
18. S. Wright, Isolation by distance. *Genetics* **28**, 114 (1943).
19. B. H. McRae, Isolation by resistance. *Evolution* **60**, 1551–1561 (2006).
20. S. Wright, Evolution in mendelian populations. *Genetics* **16**, 97 (1931).
21. J. P. Sexton, S. B. Hangartner, A. A. Hoffmann, Genetic isolation by environment or distance: Which pattern of gene flow is most common? *Evolution* **68**, 1–15 (2014).
22. L. D. Harris, G. Silva-Lopez, "Forest fragmentation and the conservation of biological diversity" in *Conservation Biology: The Theory and Practice of Nature Conservation Preservation and Management*, P. L. Fiedler, S. K. Jain, Eds. (Springer, 1992), pp. 197–237.
23. G. Greenbaum, N. H. Fefferman, Application of network methods for understanding evolutionary dynamics in discrete habitats. *Mol. Ecol.* **26**, 2850–2863 (2017).
24. R. J. Dyer, J. D. Nason, Population graphs: The graph theoretic shape of genetic structure. *Mol. Ecol.* **13**, 1713–1727 (2004).
25. A. F. Rozenfeld *et al*., Network analysis identifies weak and strong links in a metapopulation system. *Proc. Natl. Acad. Sci. U.S.A.* **105**, 18824–18829 (2008).
26. R. J. Dyer, J. D. Nason, R. C. Garrick, Landscape modelling of gene flow: Improved power using conditional genetic distance derived from the topology of population networks. *Mol. Ecol.* **19**, 3746–3759 (2010).
27. D. Petkova, J. Novembre, M. Stephens, Visualizing spatial population structure with estimated effective migration surfaces. *Nat. Genet.* **48**, 94–100 (2016).
28. J. Marcus, W. Ha, R. F. Barber, J. Novembre, Fast and flexible estimation of effective migration surfaces. *eLife* **10**, e61927 (2021).
29. I. Munwes *et al*., The change in genetic diversity down the core-edge gradient in the eastern spadefoot toad (*Pelobates syriacus*). *Mol. Ecol.* **19**, 2675–2689 (2010).
30. R. R. Marrotte *et al*., Multi-species genetic connectivity in a terrestrial habitat network. *Mov. Ecol.* **5**, 21 (2017).
31. C. J. Garroway, J. Bowman, P. J. Wilson, Using a genetic network to parameterize a landscape resistance surface for fishers, *Martes pennanti*. *Mol. Ecol.* **20**, 3978–3988 (2011).
32. P. Paschou *et al*., Maritime route of colonization of Europe. *Proc. Natl. Acad. Sci. U.S.A.* **111**, 9211–9216 (2014).
33. T. Windmaißer, S. Kattari, G. Heubl, C. Reisch, Glacial refugia and postglacial expansion of the alpine-prealpine plant species *Polygala chamaebuxus*. *Ecol. Evol.* **6**, 7809–7819 (2016).
34. M. Penrose, *Random Geometric Graphs* (OUP Oxford, 2003), vol. 5.
35. J. Dall, M. Christensen, Random geometric graphs. *Phys. Rev. E* **66**, 016121 (2002).
36. N. Alcala, A. Goldberg, U. Ramakrishnan, N. A. Rosenberg, Coalescent theory of migration network motifs. *Mol. Biol. Evol.* **36**, 2358–2374 (2019).
37. H. M. Wilkinson-Herbots, Genealogy and subpopulation differentiation under various models of population structure. *J. Math. Biol.* **37**, 535–585 (1998).
38. M. Slatkin, Inbreeding coefficients and coalescence times. *Genet. Res.* **58**, 167–175 (1991).
39. M. Kimura, Theoretical foundation of population genetics at the molecular level. *Theor. Popul. Biol.* **2**, 174–208 (1971).
40. F. A. Rodrigues, "Network centrality: an introduction" in *A Mathematical Modeling Approach from Nonlinear Dynamics to Complex Systems*, E. E. N. Macau, Ed. (Springer, 2018), pp. 177–196.
41. Y. S. Rodger, G. Greenbaum, M. Silver, S. Bar-David, G. Winters, Detecting hierarchical levels of connectivity in a population of *Acacia tortilis* at the northern edge of the species' global distribution: Combining classical population genetics and network analyses. *PLoS One* **13**, e0194901 (2018).
42. D. Eppstein, Finding the *k* shortest paths. *SIAM J. Comput.* **28**, 652–673 (1998).
43. J. D. Noh, H. Rieger, Random walks on complex networks. *Phys. Rev. Lett.* **92**, 118701 (2004).
44. M. Scheffer, S. Carpenter, J. A. Foley, C. Folke, B. Walker, Catastrophic shifts in ecosystems. *Nature* **413**, 591–596 (2001).
45. M. Scheffer *et al*., Early-warning signals for critical transitions. *Nature* **461**, 53–59 (2009).
46. V. Dakos *et al*., Methods for detecting early warnings of critical transitions in time series illustrated using simulated ecological data. *PLoS One* **7**, e41010 (2012).
47. V. Guttal, C. Jayaprakash, Changing skewness: An early warning signal of regime shifts in ecosystems. *Ecol. Lett.* **11**, 450–460 (2008).
48. A. J. Veraart *et al*., Recovery rates reflect distance to a tipping point in a living system. *Nature* **481**, 357–359 (2012).
49. I. Hanski, Habitat fragmentation and species richness. *J. Biogeogr.* **42**, 989–993 (2015).
50. D. Watson *et al*., Monitoring ecological consequences of efforts to restore landscape-scale connectivity. *Biol. Conserv.* **206**, 201–209 (2017).
51. R. Frankham, Challenges and opportunities of genetic approaches to biological conservation. *Biol. Conserv.* **143**, 1919–1927 (2010).
52. K. Riitters, J. Wickham, R. O'Neill, B. Jones, E. Smith, Global-scale patterns of forest fragmentation. *Conserv. Ecol.* **4**, 3 (2000).
53. N. Keyghobadi, J. Roland, S. Matter, C. Strobeck, Among- and within-patch components of genetic diversity respond at different rates to habitat fragmentation: An empirical demonstration. *Proc. R. Soc. B Biol. Sci.* **272**, 553–560 (2005).
54. F. W. Allendorf, Genetic drift and the loss of alleles versus heterozygosity. *Zoo Biol.* **5**, 181–190 (1986).
55. A. R. Templeton, *Population Genetics and Microevolutionary Theory* (John Wiley & Sons, 2021).
56. F. W. Allendorf, G. H. Luikart, S. N. Aitken, *Conservation and the Genetics of Populations* (John Wiley & Sons, 2012).
57. H. Andren, Effects of habitat fragmentation on birds and mammals in landscapes with different proportions of suitable habitat: A review. *Oikos* **71**, 355–366 (1994).
58. H. Andren, Population responses to habitat fragmentation: Statistical power and the random sample hypothesis. *Oikos* **76**, 235–242 (1996).
59. R. Pardini, A. Bueno, T. Gardner, P. Prado, J. Metzger, Beyond the fragmentation threshold hypothesis: Regime shifts in biodiversity across fragmented landscapes. *PLoS One* **5**, e13666 (2010).
60. A. A. Hoffmann, Y. Willi, Detecting genetic responses to environmental change. *Nat. Rev. Genet.* **9**, 421–432 (2008).

61. V. Dakos *et al*., Slowing down as an early warning signal for abrupt climate change. *Proc. Natl. Acad. Sci. U.S.A.* **105**, 14308–14312 (2008).
62. B. K. Epperson, *Geographical Genetics (MPB-38)* (Princeton University Press, 2003), vol. 38.
63. E. Crispo, A. Hendry, Does time since colonization influence isolation by distance? A meta-analysis. *Conserv. Genet.* **6**, 665–682 (2005).
64. D. G. Jenkins *et al*., A meta-analysis of isolation by distance: Relic or reference standard for landscape genetics?. *Ecography* **33**, 315–320 (2010).
65. A. Storfer, M. A. Murphy, S. F. Spear, R. Holderegger, L. P. Waits, Landscape genetics: Where are we now? *Mol. Ecol.* **19**, 3496–3514 (2010).
66. S. Ramachandran *et al*., Support from the relationship of genetic and geographic distance in human populations for a serial founder effect originating in Africa. *Proc. Natl. Acad. Sci. U.S.A.* **102**, 15942–15947 (2005).
67. B. H. McRae, P. Beier, Circuit theory predicts gene flow in plant and animal populations. *Proc. Natl. Acad. Sci. U.S.A.* **104**, 19885–19890 (2007).
68. A. Gómez-Fernández, I. Alcocer, S. Matesanz, Does higher connectivity lead to higher genetic diversity? Effects of habitat fragmentation on genetic variation and population structure in a gypsophile. *Conserv. Genet.* **17**, 631–641 (2016).
69. T. N. Wasserman, S. A. Cushman, J. S. Littell, A. J. Shirk, E. L. Landguth, Population connectivity and genetic diversity of American marten (*Martes americana*) in the United States northern Rocky Mountains in a climate change context. *Conserv. Genet.* **14**, 529–541 (2013).
70. M. Jangjoo, S. F. Matter, J. Roland, N. Keyghobadi, Connectivity rescues genetic diversity after a demographic bottleneck in a butterfly population network. *Proc. Natl. Acad. Sci. U.S.A.* **113**, 10914–10919 (2016).
71. J. T. Kool, A. Moilanen, E. A. Treml, Population connectivity: Recent advances and new perspectives. *Landsc. Ecol.* **28**, 165–185 (2013).
72. J. F. Crow, K. Aoki, Group selection for a polygenic behavioral trait: Estimating the degree of population subdivision. *Proc. Natl. Acad. Sci. U.S.A.* **81**, 6073–6077 (1984).
73. S. L. Varvio, R. Chakraborty, M. Nei, Genetic variation in subdivided populations and conservation genetics. *Heredity* **57**, 189–198 (1986).
74. M. Barthélemy, Spatial networks. *Phys. Rep.* **499**, 1–101 (2011).
75. A. Hagberg, P. J. Swart, D. A. Schult, "Exploring network structure, dynamics, and function using networkx" (Tech. Rep. LA-UR-08-05495, Los Alamos National Laboratory (LANL), Los Alamos, NM, United States, 2008).
76. L. K. Marsh, "The nature of fragmentation" in *Primates in Fragments: Ecology and Conservation*, L. K. Marsh, Ed. (Springer, 2003), pp. 1–10.
77. L. Hubert, J. Schultz, Quadratic assignment as a general data analysis strategy. *Br. J. Math. Stat. Psychol.* **29**, 190–241 (1976).
78. R. A. Fisher, *Statistical methods for research workers* (Oliver and Boyd, 1934).
79. O. Peled *et al.*, Data from: Network-based genetic monitoring of landscape fragmentation pop_net_fragmentation (code and data repository). GitHub. https://github.com/Greenbaum-Lab/pop_net_fragmentation. Deposited 1 February 2026.